Computers & Structures Vol. 26, No. 5, pp. 823–829, 1987
Printed in Great Britain.

0045-7949/87 $3.00 + 0.00

INTEGRATION OF PLASTICITY EQUATIONS FOR SINGULAR YIELD FUNCTIONS

R. DE BORST†
Department of Mechanical Engineering, University of New Mexico, Albuquerque, NM 87131, U.S.A.

(*Received* 13 *November* 1986)

Abstract—An algorithm is described which properly handles integration of stress–strain laws at singular points in a yield surface. Koiter's requirements for such points are incorporated exactly within the proposed algorithm. The conditions for which the stress, after correction for plastic flow, exactly satisfies the yield function are discussed. The algorithm is elaborated for the Mohr–Coulomb and Tresca yield criteria and an explicit expression is provided to decide whether the current regime is a corner of the yield surface or not.

1. INTRODUCTION

The predictive capability of a nonlinear analysis depends on a considerable number of factors such as the spatial discretization, the iterative solution procedure, the constitutive models, the integration of the differential stress–strain law over the loading step and so on. The impact of each of the aforementioned aspects on the accuracy should be assessed carefully in order to gain some insight in the reliability of a nonlinear analysis. A particular aspect which has received considerable attention over the past decade is the integration of the stress–strain law over the loading step, albeit that most considerations pertain to elasto-plastic solids [4, 8–16, 18].

In some respect, the history of integrators for elasto-plastic models parallels the evolution of plasticity theory, since in the literature on integrators for elasto-plasticity we also first encounter developments in metal plasticity [8, 14, 15], while contributions on frictional materials and non-associated flow rules have emerged only recently [9, 10, 13, 16].

An aspect of integration of elasto-plastic constitutive relations which so far has received only moderate attention is the treatment of singularities in a yield surface. Some popular yield functions such as the Mohr–Coulomb and the Tresca criteria possess such 'so-called' corners where the yield function is no longer continuously differentiable. Although Koiter [7] has provided a rigorous generalization of plasticity theory to accommodate such singularities, early attempts to incorporate corners in a computer program did not use Koiter's theory as a starting point, but rather aimed at rounding off the corners when the stress point was in the vicinity of a singularity [11]. However, this approach whereby the Mohr–Coulomb criterion is replaced by the Drucker–Prager criterion in the neighborhood of the corner (or alternatively the von Mises criterion is substituted for the Tresca criterion) effectively introduces new corners at the intersection of the Mohr–Coulomb and the Drucker–Prager surface. A better approach is to place a small cone in the corner such that a smooth transition between the regular part of the yield surface and this cone is obtained. However, the accuracy and stability characteristics of such a procedure where we locally have a large curvature in the yield surface are probably not good since Ortiz and Popov [12] have recently shown that a strongly curved part of the yield surface deteriorates the accuracy and stability properties.

In this paper a procedure for handling corner points in a yield surface is described which is based on Koiter's [7] generalization of the theory of the plastic potential for singular yield surfaces [1, 3]. The algorithm is rather general in the sense that non-associated flow rules are incorporated and the pressure-dependent yield functions do not pose special problems.

It is not so straightforward to classify the advocated algorithm within the framework for elasto-plastic integrators as recently developed by Ortiz and Popov [12]. This is because the algorithm essentially deploys a single-point numerical integration rule, while presently no iterations are added thereafter. Nevertheless, exact satisfaction of the yield function at the end of the loading step can be achieved for any singularity within a yield surface when a linear hardening rule is employed. Moreover, a rigorous return to the yield surface is also obtained at smooth parts of a number of commonly employed yield criteria such as Tresca, Mohr–Coulomb and von Mises, again subject to the restriction of linear hardening rules. When iterations are added, satisfaction of the yield function is also possible for more complex hardening rules and arbitrary yield functions. The algorithm may then be conceived as an Euler backward algorithm.

† On leave from TNO Institute for Building Materials and Structures, P.O. Box 49, 2600 AA Delft, The Netherlands.

2. SMOOTH PARTS OF THE YIELD SURFACE

A basic notion of small-deformation elasto-plasticity is the resolution of the total strain rate $\dot{\boldsymbol{\epsilon}}$ into an elastic component $\dot{\boldsymbol{\epsilon}}^e$, and a plastic component $\dot{\boldsymbol{\epsilon}}^p$,

$$\dot{\boldsymbol{\epsilon}} = \dot{\boldsymbol{\epsilon}}^e + \dot{\boldsymbol{\epsilon}}^p. \tag{1}$$

When we consider a material like concrete which exhibits fracture, we also have to include a fracturing strain rate $\dot{\boldsymbol{\epsilon}}^f$ owing to (micro)-cracking [3]. The elastic strain rate $\dot{\boldsymbol{\epsilon}}^e$ is assumed to be related to the stress rate $\dot{\boldsymbol{\sigma}}$ via the elasticity matrix $\boldsymbol{D}^e$,

$$\dot{\boldsymbol{\sigma}} = \boldsymbol{D}^e \dot{\boldsymbol{\epsilon}}^e. \tag{2}$$

The plastic strain rate $\dot{\boldsymbol{\epsilon}}^p$ is assumed to be derivable from a plastic potential function $g = g(\boldsymbol{\sigma}, \kappa)$ with κ some hardening parameter which is a functional of the plastic strain history, such that

$$\dot{\boldsymbol{\epsilon}}^p = \lambda \frac{\partial g}{\partial \boldsymbol{\sigma}}. \tag{3}$$

Plastic flow occurs if the yield function $f = f(\boldsymbol{\sigma}, \kappa)$ and its derivative both vanish ($f = 0$ and $\dot{f} = 0$). Elaboration of the consistency condition $\dot{f} = 0$ results in

$$\left(\frac{\partial f}{\partial \boldsymbol{\sigma}}^T\right) \dot{\boldsymbol{\sigma}} - h\lambda = 0 \tag{4}$$

with h, the hardening parameter, given by

$$h = -\frac{\partial f}{d\kappa} \left(\frac{\partial \kappa}{\partial \boldsymbol{\epsilon}^p}\right)^T \frac{\partial g}{\partial \boldsymbol{\sigma}}. \tag{5}$$

The superscript T in eqns (4) and (5) is used to denote a transpose. Combining eqns (1)–(4) yields the tangential relation between stress rates and strain rates

$$\dot{\boldsymbol{\sigma}} = \left[\boldsymbol{D}^e - \frac{\boldsymbol{D}^e (\partial g/\partial \boldsymbol{\sigma})/(\partial f/\partial \boldsymbol{\sigma})^T \boldsymbol{D}^e}{h + (\partial f/\partial \boldsymbol{\sigma})^T \boldsymbol{D}^e (\partial g/\partial \boldsymbol{\sigma})}\right] \dot{\boldsymbol{\epsilon}}. \tag{6}$$

It is noted that explicit distinction is made between a yield function f and a plastic potential function g. This implies that non-associated flow rules may be included.

Integrating eqn (6) we obtain for a finite stress increment

$$\Delta \boldsymbol{\sigma} = \int_{t-\Delta t}^{t} \left[\boldsymbol{D}^e - \frac{\boldsymbol{D}^e (\partial g/\partial \boldsymbol{\sigma})/(\partial f/\partial \boldsymbol{\sigma})^T \boldsymbol{D}^e}{h + (\partial f/\partial \boldsymbol{\sigma})^T \boldsymbol{D}^e (\partial g/\partial \boldsymbol{\sigma})}\right] \dot{\boldsymbol{\epsilon}} \, d\tau. \tag{7}$$

All algorithms for handling the integral of eqn (7) basically consist of two parts. In the first part, a trial stress increment $\Delta \boldsymbol{\sigma}^t$ is computed, while a correction for inelastic behavior is made in a corrector phase. Since the material is assumed to behave fully elastically in the predictor phase, we have the identities

$$\boldsymbol{D}^e \dot{\boldsymbol{\epsilon}} = \dot{\boldsymbol{\sigma}}^t \tag{8}$$

$$\left(\frac{\partial f}{\partial \boldsymbol{\sigma}}\right)^T \dot{\boldsymbol{\sigma}}^t = \dot{f}^t \tag{9}$$

so that we can write eqn (7) as

$$\Delta \boldsymbol{\sigma} = \int_{t-\Delta t}^{t} \left[\dot{\boldsymbol{\sigma}}^t - \frac{\dot{f}^t \boldsymbol{D}^e (\partial g/\partial \boldsymbol{\sigma})}{h} + (\partial f/\partial \boldsymbol{\sigma})^T \boldsymbol{D}^e (\partial g/\partial \boldsymbol{\sigma})\right] d\tau. \tag{10}$$

Introducing the notation

$$\boldsymbol{\sigma}^t = \boldsymbol{\sigma}^0 + \Delta \boldsymbol{\sigma}^t \tag{11}$$

with $\boldsymbol{\sigma}^0$ either the contact stress at the intersection of the stress path and the yield surface or the stress at the beginning of the loading step (Fig. 1), we obtain, with a single-point numerical integration rule,

$$\Delta \boldsymbol{\sigma} = \Delta \boldsymbol{\sigma}^t - \frac{f(\boldsymbol{\sigma}^t, \kappa^0)}{h + (\partial f/\partial \boldsymbol{\sigma})^T \boldsymbol{D}^e (\partial g/\partial \boldsymbol{\sigma})} \boldsymbol{D}^e \frac{\partial g}{\partial \boldsymbol{\sigma}}, \tag{12}$$

since by definition we have $f(\boldsymbol{\sigma}^0, \kappa^0) = 0$. Numerically, the condition $f(\boldsymbol{\sigma}^0, \kappa^0) = 0$ need not be satisfied because the stresses resulting from a previous loading step may violate the yield function slightly. By putting $f(\boldsymbol{\sigma}^0, \kappa^0) = 0$ we strive to satisfy the yield criterion at any stage of the loading process, so that inaccuracies from previous loading steps are not carried along.

The approach becomes very simple if the gradients to the yield function f and the plastic potential g are evaluated for $\boldsymbol{\sigma} = \boldsymbol{\sigma}^t$. Then, there is no need to determine the intersection point of the stress path with the yield function. Especially with complicated yield functions, or when fracturing of concrete or rock is also included in the analysis, evaluation of the gradients at $\boldsymbol{\sigma} = \boldsymbol{\sigma}^t$ may simplify the computer code significantly. Here, it is appropriate to remark that simplicity is of paramount importance to large, general purpose finite element codes, and it may sometimes be justifiable to sacrifice accuracy (but not, of course, stability and robustness!) to keep the computer code relatively simple.

It is also interesting to note that for the particular case that the gradients are evaluated at $\boldsymbol{\sigma} = \boldsymbol{\sigma}^t$ the approach reduces to the elastic predictor–radial return scheme for an associated von Mises plasticity model [3]. Also, the implicit Euler backward algorithm for a Drucker–Prager yield function described recently by Loret and Prévost [9] is contained in

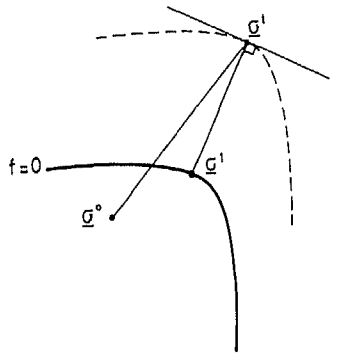

Fig. 1. Stress correction for plasticity.

eqn (12) since when we substitute that yield function in eqn (12) we recover their equations. The above observations support the assertion that the approach described in the preceding is probably very competitive amongst the single-point integrators, since for a von Mises solid [8, 15] and for a Drucker–Prager solid [9] this scheme has been shown to be highly accurate.

3. SINGULARITIES IN THE YIELD SURFACE

A major advantage of the scheme discussed in the preceding section is the ease with which singularities which occur in Mohr–Coulomb type yield functions can be dealt. These singularities occur when two principal stresses become equal. Koiter [7] has shown that when, in fact, two yield functions are active, the plastic strain rate can be written as

$$\dot{\epsilon}^p = \lambda_1 \frac{\partial g_1}{\partial \sigma} + \lambda_2 \frac{\partial g_2}{\partial \sigma}, \tag{13}$$

where g_1 and g_2 are the plastic potential functions which belong to the yield functions which are active (f_1 and f_2, Fig. 2). We observe that we now have two non-negative multipliers (λ_1 and λ_2) instead of only one non-negative plastic multiplier.

We suppose that during an infinitesimally small increment the stress point remains in the corner of the yield surface. It will be shown in the next section for the Mohr–Coulomb criterion how it can be determined whether this condition indeed holds for finite increments. When the stress point remains in a singular point of the yield surface the consistency condition for the first as well as for the second yield function must be satisfied.

$$\dot{f}_1 = 0 \quad \text{and} \quad \dot{f}_2 = 0. \tag{14}$$

Using eqn (13) these conditions can be elaborated as

$$\left(\frac{\partial f_1}{\partial \sigma}\right)^T \dot{\sigma} + \frac{\partial f_1}{\partial \kappa}\left(\frac{\partial \kappa}{\partial \epsilon^p}\right)^T \left(\lambda_1 \frac{\partial g_1}{\partial \sigma} + \lambda_2 \frac{\partial g_2}{\partial \sigma}\right) = 0 \tag{15}$$

$$\left(\frac{\partial f_2}{\partial \sigma}\right)^T \dot{\sigma} + \frac{\partial f_2}{\partial \kappa}\left(\frac{\partial \kappa}{\partial \epsilon^p}\right)^T \left(\lambda_1 \frac{\partial g_1}{\partial \sigma} + \lambda_2 \frac{\partial g_2}{\partial \sigma}\right) = 0. \tag{16}$$

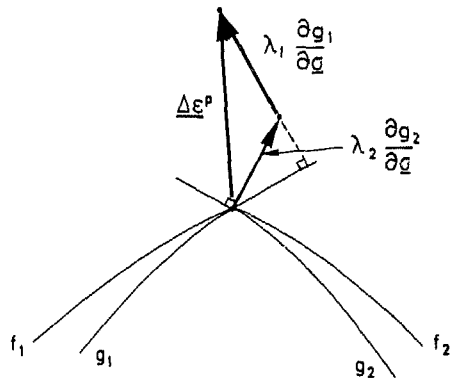

Fig. 2. Plastic flow at a singularity in the yield surface.

We next combine the flow rule at a singularity (13), the resolution of strain rates (1) and the elasticity relation (2). This results in:

$$\dot{\sigma} = \boldsymbol{D}^e\left(\dot{\epsilon} - \lambda_1 \frac{\partial g_1}{\partial \sigma} - \lambda_2 \frac{\partial g_2}{\partial \sigma}\right). \tag{17}$$

Premultiplying eqn (17) with the gradients to f_1 and f_2 and invoking eqns (15) and (16) yields

$$\mu_1 \lambda_1 + \mu_2 \lambda_2 = \left(\frac{\partial f_1}{\partial \sigma}\right)^T \boldsymbol{D}^e \dot{\epsilon} \tag{18}$$

$$\mu_3 \lambda_1 + \mu_4 \lambda_2 = \left(\frac{\partial f_2}{\partial \sigma}\right)^T \boldsymbol{D}^e \dot{\epsilon} \tag{19}$$

where μ_1, μ_2, μ_3, μ_4 are defined as

$$\mu_1 = \left(-\frac{\partial f_1}{\partial \kappa}\frac{\partial \kappa}{\partial \epsilon^p} + \boldsymbol{D}^e \frac{\partial f_1}{\partial \sigma}\right)^T \frac{\partial g_1}{\partial \sigma} \tag{20}$$

$$\mu_2 = \left(-\frac{\partial f_1}{\partial \kappa}\frac{\partial \kappa}{\partial \epsilon^p} + \boldsymbol{D}^e \frac{\partial f_1}{\partial \sigma}\right)^T \frac{\partial g_2}{\partial \sigma} \tag{21}$$

$$\mu_3 = \left(-\frac{\partial f_2}{\partial \kappa}\frac{\partial \kappa}{\partial \epsilon^p} + \boldsymbol{D}^e \frac{\partial f_2}{\partial \sigma}\right)^T \frac{\partial g_1}{\partial \sigma} \tag{22}$$

$$\mu_4 = \left(-\frac{\partial f_2}{\partial \kappa}\frac{\partial \kappa}{\partial \epsilon^p} + \boldsymbol{D}^e \frac{\partial f_2}{\partial \sigma}\right)^T \frac{\partial g_2}{\partial \sigma}. \tag{23}$$

Solving the set of eqns (18) and (19) for λ_1 and λ_2 gives

$$\lambda_1 = \frac{\mu_4 (\partial f_1/\partial \sigma)^T \boldsymbol{D}^e \dot{\epsilon} - \mu_2 (\partial f_2/\partial \sigma)^T \boldsymbol{D}^e \dot{\epsilon}}{\mu_1 \mu_4 - \mu_2 \mu_3} \tag{24}$$

$$\lambda_2 = \frac{\mu_1 (\partial f_2/\partial \sigma)^T \boldsymbol{D}^e \dot{\epsilon} - \mu_3 (\partial f_1/\partial \sigma)^T \boldsymbol{D}^e \dot{\epsilon}}{\mu_1 \mu_4 - \mu_2 \mu_3} \tag{25}$$

so that we obtain for the rate equation

$$\dot{\sigma} = \left\{ \boldsymbol{D}^e - \frac{\boldsymbol{D}^e\left[\mu_1 \frac{\partial g_2}{\partial \sigma}\left(\frac{\partial f_2}{\partial \sigma}\right)^T + \mu_4 \frac{\partial g_1}{\partial \sigma}\left(\frac{\partial f_1}{\partial \sigma}\right)^T\right]\boldsymbol{D}^e}{\mu_1 \mu_4 - \mu_2 \mu_3} + \frac{\boldsymbol{D}^e\left[\mu_2 \frac{\partial g_1}{\partial \sigma}\left(\frac{\partial f_2}{\partial \sigma}\right)^T + \mu_3 \frac{\partial g_2}{\partial \sigma}\left(\frac{\partial f_1}{\partial \sigma}\right)^T\right]\boldsymbol{D}^e}{\mu_1 \mu_4 - \mu_2 \mu_3} \right\} \dot{\epsilon}. \tag{26}$$

For integration to finite strain and stress increments we again utilize the trial stress rate $\dot{\sigma}'$ from eqn (8) and the relations

$$\left(\frac{\partial f_1}{\partial \sigma}\right)^T \dot{\sigma}' = \dot{f}_1 \tag{27}$$

$$\left(\frac{\partial f_2}{\partial \sigma}\right)^T \dot{\sigma}' = \dot{f}_2 \tag{28}$$

which are valid during the calculation of the test stress increment $\Delta\sigma'$ because no plastic flow is assumed to occur during this phase. Inserting eqns (27) and (28)

in eqn (26) and integrating over a finite load step yields

$$\Delta\boldsymbol{\sigma} = \int_{t-\Delta t}^{t} \left\{ \dot{\boldsymbol{\sigma}}^t - \frac{(\mu_4 \dot{f}_1 - \mu_2 \dot{f}_2)\boldsymbol{D}^e(\partial g_1/\partial\boldsymbol{\sigma})}{\mu_1\mu_4 - \mu_2\mu_3} - \frac{(\mu_1 \dot{f}_2 - \mu_3 \dot{f}_1)\boldsymbol{D}^e(\partial g_2/\partial\boldsymbol{\sigma})}{\mu_1\mu_4 - \mu_2\mu_3} \right\} \mathrm{d}\tau \quad (29)$$

or with a single-point numerical integration rule

$$\Delta\boldsymbol{\sigma} = \Delta\boldsymbol{\sigma}^t - \frac{\mu_4 f_1(\boldsymbol{\sigma}^t, \kappa^0) - \mu_2 f_2(\boldsymbol{\sigma}^t, \kappa^0)}{\mu_1\mu_4 - \mu_2\mu_3} \boldsymbol{D}^e \frac{\partial g_1}{\partial\boldsymbol{\sigma}} - \frac{\mu_1 f_2(\boldsymbol{\sigma}^t, \kappa^0) - \mu_3 f_1(\boldsymbol{\sigma}^t, \kappa^0)}{\mu_1\mu_4 - \mu_2\mu_3} \boldsymbol{D}^e \frac{\partial g_2}{\partial\boldsymbol{\sigma}}. \quad (30)$$

Another way of looking at the above procedure is that after the calculation of the test stress increment $\Delta\boldsymbol{\sigma}^t$ a correction must be applied such that the final stress state $\boldsymbol{\sigma}^1$ complies with both yield functions, i.e. $f_1(\boldsymbol{\sigma}^1, \kappa^1) = 0$ and $f_2(\boldsymbol{\sigma}^1, \kappa^1) = 0$. Using the notion that

$$\boldsymbol{\sigma}^1 = \boldsymbol{\sigma}^t - \boldsymbol{D}^e \Delta\boldsymbol{\epsilon}^p \quad (31)$$

and using the flow rule at a singularity then yields

$$f_1\left(\boldsymbol{\sigma}^t - \lambda_1 \frac{\partial g_1}{\partial\boldsymbol{\sigma}} - \lambda_2 \frac{\partial g_2}{\partial\boldsymbol{\sigma}}, \kappa^1\right) = 0 \quad (32)$$

$$f_2\left(\boldsymbol{\sigma}^t - \lambda_1 \frac{\partial g_1}{\partial\boldsymbol{\sigma}} - \lambda_2 \frac{\partial g_2}{\partial\boldsymbol{\sigma}}, \kappa^1\right) = 0 \quad (33)$$

whereupon expansion in a Taylor series around $\boldsymbol{\sigma} = \boldsymbol{\sigma}^t$, $\kappa = \kappa^0$ and discarding the quadratic and higher-order terms precisely yields eqn (30).

In this expansion only the linear terms have been retained. With respect to the yield surface this is no limitation, since any yield function may be linearized around a singularity without loss of generality (Fig. 2). With respect to the dependence of the yield function on the hardening parameter κ, neglecting higher-order terms means that the treatment is only exact for linear-hardening solids. Furthermore, the assumption has been made implicitly that $\dot{\kappa}$ is a linear function of the plastic strain rate $\dot{\boldsymbol{\epsilon}}^p$, which is not valid for a number of important hardening hypotheses like, for instance, the strain-hardening hypothesis. For regular parts of the yield surface, the nonlinear dependence of $\dot{\kappa}$ on $\dot{\boldsymbol{\epsilon}}^p$ does not entail errors, but for the corner regimes an additional error is introduced. If these errors cannot be tolerated, the stress $\boldsymbol{\sigma}^1 = \boldsymbol{\sigma}^0 + \Delta\boldsymbol{\sigma}$, with the stress increment following from eqn (30), can be used as a first estimate in an iterative procedure which yields an improved estimate for $\boldsymbol{\sigma}^1$.

It is noted that the above limitations also hold for regular parts of the yield surface. In fact, the restrictions may then be more stringent since the yield function generally shows a nonlinear dependence on the stresses. Consequently, an iterative procedure is necessary but for yield functions which linearly depend on stress (Mohr–Coulomb and Tresca), and some special cases of the Drucker-Prager yield function (see e.g. [9]).

Most approaches which are currently used for handling singularities in yield surfaces are based on rounding off the corners (e.g. [11]). Another procedure based on Koiter's generalization [7] has been proposed by Marques [10]. There are some major differences between Marques' approach and the algorithm presented here. First, Marques' approach is of an explicit nature while the method advocated here is implicit. This has definite advantages with regard to satisfying the yield function. More serious, however, is that Marques' elaboration of the consistency conditions at a singularity is not correct and definitely does not coincide with eqns (15) and (16) derived here.

4. MOHR–COULOMB TYPE YIELD FUNCTIONS

The Mohr–Coulomb yield function is defined by

$$f = \tfrac{1}{2}(\sigma_3 - \sigma_1) + \tfrac{1}{2}(\sigma_3 + \sigma_1)\sin\phi_m - c_m, \quad (34)$$

where

$$\sigma_3 \geqslant \sigma_2 \geqslant \sigma_1, \quad (35)$$

ϕ_m is the mobilized friction angle which may be some function of the hardening parameter κ, and c_m is the mobilized cohesion which may also be a function of κ. A plastic potential function g can be defined in a similar fashion as the yield function f but for replacement of the mobilized friction angle ϕ_m by a mobilized dilatancy angle ψ_m [17]:

$$g = \tfrac{1}{2}(\sigma_3 - \sigma_1) + \tfrac{1}{2}(\sigma_3 + \sigma_1)\sin\psi_m - c_m. \quad (36)$$

For a three-dimensional stress state, the principal stresses can be found as the roots of the cubic equation

$$\sigma^3 - I_1\sigma_2 + I_2\sigma - I_3 = 0 \quad (37)$$

with I_1, I_2 and I_3 the stress invariants (e.g. [6]). Using the deviatoric stress invariants J_2 and J_3 [6], we may replace eqn (37) by:

$$s^3 - J_2 s - J_3 = 0 \quad (38)$$

as the first deviatoric stress invariant vanishes by definition. The notation s is employed to denote deviatoric stresses. Equation (38) can be solved using Cardano's formulae. For the case of three real roots (which holds true because of the symmetry of the stress tensor), they read:

$$\begin{bmatrix} s_1 \\ s_2 \\ s_3 \end{bmatrix} = 2\sqrt{(\tfrac{1}{3}J_2)} \begin{bmatrix} \sin(\alpha - \frac{2}{3}\pi) \\ \sin\alpha \\ \sin(\alpha + \frac{2}{3}\pi) \end{bmatrix}, \quad (39)$$

where α follows from

$$\sin(3\alpha) = -\tfrac{3}{2}\sqrt{3}\frac{J_3}{J_2\sqrt{J_2}}. \quad (40)$$

Hence, we obtain for the total principal stresses:

$$\begin{bmatrix}\sigma_1\\ \sigma_2\\ \sigma_3\end{bmatrix} = 2\sqrt{(\tfrac{1}{3}J_2)}\begin{bmatrix}\sin(\alpha-\tfrac{2}{3}\pi)\\ \sin\alpha\\ \sin(\alpha+\tfrac{2}{3}\pi)\end{bmatrix} + p\begin{bmatrix}1\\1\\1\end{bmatrix} \quad (41)$$

with $p = \frac{1}{3}I_1$.

We next assume that we have the situation in which the strict inequality signs of eqns (35) hold. Then, we may substitute the expressions (41) for σ_1 and σ_3 in eqn (34). This yields:

$$f = \sqrt{J_2}\cos\alpha - [2\sqrt{(\tfrac{1}{3}J_2)} - p]\sin\phi_m - c_m \quad (42)$$

so that we have for the gradient to the yield surface:

$$\frac{df}{\partial\boldsymbol{\sigma}} = \sin\phi_m\frac{\partial p}{\partial\boldsymbol{\sigma}} + \left(a + b\frac{\partial\alpha}{\partial J_2}\right)\frac{\partial J_2}{\partial\boldsymbol{\sigma}} + b\frac{\partial\alpha}{\partial J_3}\frac{\partial J_3}{\partial\boldsymbol{\sigma}} \quad (43)$$

with the scalars a and b given by

$$a = \frac{1}{2\sqrt{J_2}}[\cos\alpha - \sqrt{\tfrac{1}{3}}\sin\alpha\sin\phi_m] \quad (44)$$

and

$$b = -\sqrt{J_2}[\sin\alpha + \sqrt{\tfrac{1}{3}}\cos\alpha\sin\phi_m]. \quad (45)$$

The manner in which the gradient to the plastic potential function g is computed, is essentially similar to the computation of the gradient to the yield function f, but for replacement of the mobilized friction angle ϕ_m by the mobilized dilatancy angle ψ_m.

When the strict inequality signs of eqn (35) do not hold, i.e. if two principal stresses become equal, the stress point is in a ridge of the Mohr–Coulomb yield surface (Fig. 3). In such a point, the yield function f is continuous, but not continuously differentiable and the plastic strain rate is determined via Koiter's generalization (13). For the Mohr–Coulomb surface, Fig. 4 shows that we essentially have two yield corners when we order the principal stresses according to eqn (35). Furthermore, the yield function (34) is active for all cases, either at a smooth part of the yield surface, or at a singularity. Hence, one of the two required gradients to the yield surface is given by eqns (43)–(45).

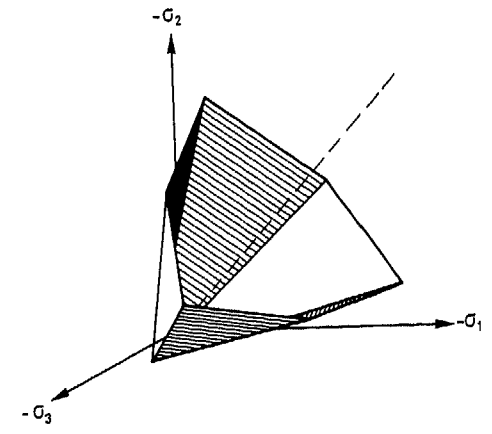

Fig. 3. Mohr–Coulomb surface in three-dimensional stress space.

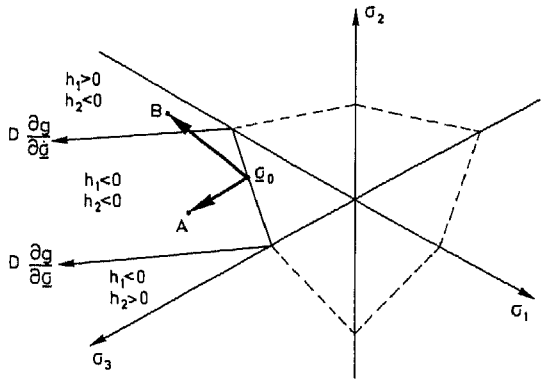

Fig. 4. Active part of Mohr–Coulomb surface in the π-plane.

Let us first suppose that we have the case in which $\sigma_1 = \sigma_2$, so that the yield function

$$f = \tfrac{1}{2}(\sigma_3 - \sigma_2) + \tfrac{1}{2}(\sigma_3 + \sigma_2)\sin\phi_m - c_m \quad (46)$$

is also active. Substituting eqn (41) for the principal stresses, and differentiating again results in eqn (43) for the gradient $\partial f/\partial\boldsymbol{\sigma}$, but now the scalars a and b are given by:

$$a = \frac{1}{4\sqrt{J_2}}\{\cos\alpha - \sqrt{3}\sin\alpha + [\sqrt{\tfrac{1}{3}}\sin\alpha + \cos\alpha]\sin\phi_m\} \quad (47)$$

and

$$b = \tfrac{1}{2}\sqrt{J_2}\{-\sin\alpha - \sqrt{3}\cos\alpha + [\sqrt{\tfrac{1}{3}}\cos\alpha - \sin\alpha]\sin\phi_m\}. \quad (48)$$

Similarly, for $\sigma_2 = \sigma_3$, we obtain

$$a = \frac{1}{4\sqrt{J_2}}\{\sin\alpha + \sqrt{3}\cos\alpha + [\sqrt{\tfrac{1}{3}}\sin\alpha - \cos\alpha]\sin\phi_m\} \quad (49)$$

and

$$b = \tfrac{1}{2}\sqrt{J_2}\{-\sin\alpha + \sqrt{3}\cos\alpha + [\sqrt{\tfrac{1}{3}}\cos\alpha + \sin\alpha]\sin\phi_m\}. \quad (50)$$

The gradients to the plastic potential are again determined in a similar fashion, by substituting the mobilized dilatancy angle ψ_m for the mobilized friction angle ϕ_m.

Finally, it has to be determined whether the trial stress is such that we have a corner regime or whether the stress correction can be calculated for a regular part of the yield surface. Figure 4 shows two trial stress points, A and B. It is evident that for point A a flow rule in the sense of eqn (3) can be used, but that for point B, application of such a rule would lead to a final stress lying outside of the yield surface, so that in the latter case we have to apply Koiter's generalization for the flow rule. The selection of the

precise flow equation might be made on basis of trial and error, but a more simple and elegant procedure has been adopted in the present study. If we have perfect plasticity, the yield surface remains fixed, so that the position of the corner point is uniquely determined in stress space. It is then easy to analytically determine a plane which passes through the corner points and which has the direction

$$\boldsymbol{D}^e \frac{\partial g}{\partial \boldsymbol{\sigma}}.$$

The projections of these vectors on the π-plane are plotted in Fig. 4. The derivation of an analytical expression for these planes is straightforward and it can be derived that if

$$h_1 < 0 \quad \text{and} \quad h_2 < 0 \tag{51}$$

we are on a regular part of the yield surface. In it, h_1 and h_2 are defined as

$$h_1 = f(\boldsymbol{\sigma}^t, \kappa^0) + \frac{1 - 2\nu + \sin\phi_m \sin\psi_m}{1 - 2\nu - (1 + 2\nu)\sin\psi_m}(\sigma_2 - \sigma_3) \tag{52}$$

and

$$h_2 = f(\boldsymbol{\sigma}^t, \kappa^0) - \frac{1 - 2\nu + \sin\phi_m \sin\psi_m}{1 - 2\nu - (1 + 2\nu)\sin\psi_m}(\sigma_2 - \sigma_1). \tag{53}$$

If we have the situation

$$h_1 > 0 \quad \text{and} \quad h_2 < 0 \tag{54}$$

we are in a corner regime for $\sigma_2 = \sigma_3$, whereas

$$h_1 < 0 \quad \text{and} \quad h_2 > 0 \tag{55}$$

defines a corner regime for $\sigma_2 = \sigma_1$. For hardening plasticity, this procedure can not rigorously predict the correct regime, because the position of the yield surface is unknown. In particular, we may erroneously arrive at the conclusion that we have a corner regime for hardening plasticity or that we have a smooth regime when we have softening. Mostly, the prediction on basis of eqns (51)–(55) will be adequate, but if necessary an *a posteriori* check may be performed so that the erroneous assumption can be corrected.

A particular problem is sometimes said to arise if two principal stresses of the trial stress become exactly equal, since the derivatives $\partial\alpha/\partial J_2$ and $\partial\alpha/\partial J_3$ would then become indeterminate. However, in practice no difficulties are encountered, as even when two principal stresses are exactly equal, the entire expression (43) for the gradient remains determinate. Actually, the gradient to the Mohr–Coulomb yield surface becomes identical to the gradient to the Drucker–Prager yield surface for this limiting case. Consider for instance the case that $\alpha = \frac{1}{6}\pi$. Then

$$\begin{bmatrix}\sigma_1\\ \sigma_2\\ \sigma_3\end{bmatrix} = \sqrt{(\tfrac{1}{3}J_2)}\begin{bmatrix}-2\\ 1\\ 1\end{bmatrix} + p\begin{bmatrix}1\\ 1\\ 1\end{bmatrix} \tag{56}$$

which upon substitution in the yield function (34) gives

$$f = \frac{3 - \sin\phi_m}{2}\sqrt{(\tfrac{1}{3}J_2)} + p\sin\phi_m. \tag{57}$$

Differentiation then results in

$$\frac{\partial f}{\partial \boldsymbol{\sigma}} = \sin\phi_m \frac{\partial p}{\partial \boldsymbol{\sigma}} + \frac{3 - \sin\phi_m}{4\sqrt{(3J_2)}}\frac{\partial J_2}{\partial \boldsymbol{\sigma}} \tag{58}$$

which is precisely the gradient which is obtained when we differentiate the Drucker–Prager yield function.

It is finally remarked that another singularity in the Mohr–Coulomb yield surface occurs at the apex of the yield cone. In fact, the numerical algorithm should check whether the stress is beyond the apex. If this happens to be the case, an additional correction should be applied to bring the stress point back to the apex of the yield cone. This problem only arises for cohesionless materials such as sand, because for cohesive materials, a fracture criterion should bound the allowable tensile stresses.

5. EXAMPLE

As an example problem we will consider axisymmetric indentation of a subsoil which is governed by a non-hardening Mohr–Coulomb elasto-plastic model (Fig. 5). The soil has been modeled as weightless and has been assumed to possess both cohesion and friction.

Analytical plasticity solutions for axisymmetric problems are usually obtained with use of the Haar–von Kármán hypothesis which postulates that at failure two principal stresses are equal [5]. If this hypothesis is valid for the present example, the problem is rather critical with regard to singularities in the yield surface.

The results in Fig. 5, which have been obtained for an associated ($\phi = \psi = 20°$) as well as a non-associated flow rule ($\phi = 20°, \psi = 0°$), show a close agreement with the analytical limit load by Cox *et al.* [5]. Moreover, the numerically calculated stress distribution at failure underneath the footing [1] also agreed closely with the analytical calculations [5] based on the Haar–von Kármán hypothesis. Indeed, the numerical calculations showed that at failure, two principal stresses were equal in virtually all integration points in which plastic deformations occurred. Consequently, the stress point was in a corner of the Mohr–Coulomb surface for a considerable number of integration points. It appeared that in all of these sampling points both active yield functions were identically satisfied.

It is perhaps somewhat surprising that the calculations for the non-associated flow rule also yielded the analytical failure load. The present problem however is not critical with regard to non-uniqueness of the limit load because of the small number of kinematic constraints and the moderate degree of non-normality [2, 3].

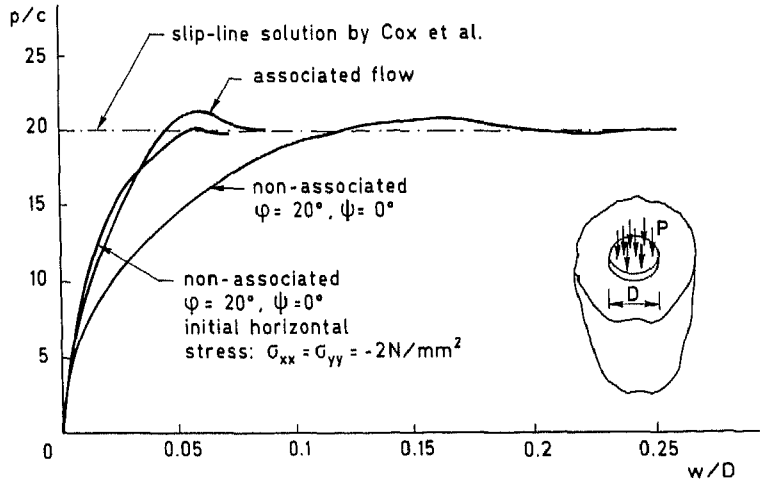

Fig. 5. Load–settlement curve for a circular footing on a cohesive-frictional soil. Two calculations have been started from a stress-free state while the third calculation was started from a non-zero horizontal stress field.

6. CONCLUSIONS

An algorithm has been proposed which properly handles corners in a yield surface [1, 3]. Unlike some previous approaches it is based on Koiter's formulation for such singularities [7]. It is general in the sense that non-associated flow rules and pressure-dependent yield functions can be handled in a straightforward fashion.

The algorithm is simple which has advantages when nonlinear phenomena other than plasticity have to be included in the analysis as well. Nevertheless, under some restrictions both yield functions which are active at such a singularity are exactly satisfied after stress correction. The restrictions for which this favorable property holds have been discussed.

The algorithm has been elaborated for the Mohr–Coulomb and the Tresca yield functions. A simple function has been introduced which determines whether a trial stress is in a corner regime or not.

Acknowledgements—The example reported in this paper has been calculated with the DIANA finite element code on the VAX 11/780 computer of the TNO Institute for Building Materials and Structures. Major parts of the research reported in this paper have been assisted financially by CUR-Committee A26 'Concrete Mechanics'.

REFERENCES

1. R. de Borst, Calculation of collapse loads using higher order elements. In: *Proc. IUTAM Symp. Deformation and Failure of Granular Materials* (Edited by P. A. Vermeer and H. J. Luger), pp. 503–513. Balkema Publ., Rotterdam (1982).
2. R. de Borst and P. A. Vermeer, Possibilities and limitations of finite elements for limit analysis. *Géotechnique* **34**, 199–210 (1984).
3. R. de Borst, Nonlinear analysis of frictional materials. Dissertation, Delft University of Technology, Delft (1986).
4. D. Bushnell, A strategy for the solution of problems involving large deflections, plasticity and creep. *Int. J. Numer. Meth. Engng* **11**, 682–708 (1977).
5. A. D. Cox, G. Eason and H. G. Hopkins, Axially symmetric plastic deformations in soils. *Phil. Trans. Roy. Soc. A* **254**, 1–47 (1961).
6. Y. C. Fung, *Foundations of Solid Mechanics*. Prentice-Hall, Englewood Cliffs, New Jersey (1965).
7. W. T. Koiter, Stress–strain relations, uniqueness and variational theorems for elastic–plastic materials with a singular yield surface. *Q. Appl. Math.* **11**, 350–354 (1953).
8. R. D. Krieg and D. B. Krieg, Accuracies of numerical solution methods for the elastic-perfectly plastic model. *J. Pressure Vessel Technol.* **99**, 510–515 (1977).
9. B. Loret and J. H. Prévost, Accurate numerical solutions for Drucker–Prager elastic–plastic models. *Comp. Meth. Appl. Mech. Engng* **54**, 259–277 (1986).
10. J. M. M. C. Marques, Stress computation in elasto-plasticity. *Engng Comput.* **1**, 42–51 (1984).
11. G. C. Nayak and O. C. Zienkiewicz, Elasto-plastic stress analysis. A generalisation for various constitutive relations including strain softening. *Int. J. Numer. Meth. Engng* **5**, 113–135 (1972).
12. M. Ortiz and E. P. Popov, Accuracy and stability of integration algorithms for elastoplastic constitutive relations. *Int. J. Numer. Meth. Engng* **21**, 1561–1576 (1985).
13. M. Ortiz and J. C. Simo, An analysis of a new class of integration algorithms for elastoplastic constitutive relations. *Int. J. Numer. Meth. Engng* **23**, 353–366 (1986).
14. J. R. Rice and D. M. Tracey, Computational fracture mechanics. In: *Proc. Symp. on Num. and Comp. Meth. in Struct. Mech.* (Edited by S. J. Fenves *et al.*), pp. 585–624. Academic Press, New York (1971).
15. H. L. Schreyer, R. F. Kulak and J. M. Kramer, Accurate numerical solution for elasto-plastic models. *J. Pressure Vessel Technol.* **101**, 226–234 (1979).
16. P. A. Vermeer, A modified initial strain method for plasticity problems. In: *Proc. Third Int. Conf. Numer. Meth. Geomech.* (Edited by W. Wittke), pp. 377–387. Balkema Publ., Rotterdam (1979).
17. P. A. Vermeer and R. de Borst, Non-associated plasticity for soils, concrete and rock. *Heron* **29**, (3) (1984).
18. P. J. Yoder and R. G. Whirley, On the numerical implementation of elastoplastic models. *J. Appl. Mech.* **51**, 283–288 (1984).